Research article

Danggui-Shaoyao-San protects against non-alcoholic steatohepatitis via modulation of hepatic APP protein, Lysosomal CTSB release, and NF-κB activation

Siting Gao [a,1], Ziming An [a,1], Qian Zhang [a,b,1], Qinmei Sun [a], Qian Huang [a], Lei Shi [c], Wei Liu [a,e], Xiaojun Gou [d], Yajuan Li [b,***], Xin Xin [e,**], Qin Feng [a,e,f,g,*]

[a] Institute of Liver Diseases, Shuguang Hospital Affiliated to Shanghai University of Traditional Chinese Medicine, Shanghai, China
[b] Institute of Interdisciplinary Integrative Medicine Research, Shanghai University of Traditional Chinese Medicine, Shanghai, China
[c] Department of Clinical Laboratory, Shuguang Hospital Affiliated to Shanghai University of Traditional Chinese Medicine, Shanghai, China
[d] Central Laboratory, Baoshan District Hospital of Integrated Traditional Chinese and Western Medicine of Shanghai, Shanghai, China
[e] Key Laboratory of Liver and Kidney Diseases, Shanghai University of Traditional Chinese Medicine, Ministry of Education, Shanghai, China
[f] Central Laboratory, ShuGuang Hospital Affiliated to Shanghai University of Chinese Traditional Medicine, Shanghai, China
[g] Shanghai Key Laboratory of Traditional Chinese Clinical Medicine, Shanghai, China

A B S T R A C T

Background: Non-alcoholic steatohepatitis (NASH), an escalating global health concern, is a primary factor behind cirrhosis, liver transplantation, and hepatocellular carcinoma. Effective treatments remain elusive. Danggui-Shaoyao-San (DGSY), a classic famous prescription employed in treating NASH, could hold promise, although its molecular underpinnings are still under investigation. This study undertakes an exploration of the impacts of DGSY on NASH and seeks to illuminate the mechanisms at play.
Methods: UHPLC-Q-Orbitrap HRMS was employed to identify compounds within DGSY. Mice underwent a 25-week regimen of HFHC diet and high-sugar water, with 4 weeks of DGSY treatment for efficacy and pathogenic mechanism exploration *in vivo*. L02 cells were cultured with 0.2 mM FFA for 24 h, exposed to DGSY at 1 mg/ml and 2 mg/ml for efficacy and pathogenic mechanism exploration in *vitro*. Using online databases, we sought potential targets for NASH treatment, and through PPI networks, identified key targets. Expression levels of genes and proteins were examined by western blotting, RT-PCR, and immunofluorescence staining.
Results: Thirty-four compounds were identified within DGSY. DGSY brought about marked reductions in biochemical indicators and yielded significant improvements in NASH mice histological features. Additionally, it mitigated hepatic steatosis and inflammation both *in vivo* and *in vitro*. The top 10 targets from two network pharmacology analyses, one focusing on structural prediction and the other on literature mining, identified APOE and APP as potential therapeutic targets for DGSY in NASH treatment. PCR validation confirmed that DGSY reduced APP expression after treatment, and further investigation revealed that DGSY significantly suppressed

* Corresponding author. 528 Zhangheng Road, Pudong New Area, Shanghai, 201210, China.
** Corresponding author. 528 Zhangheng Road, Pudong New Area, Shanghai, 201210, China.
*** Corresponding author. 1200 Cailun Road, Pudong New Area, Shanghai, 201203, China.
E-mail addresses: liyajuan9@sina.cn (Y. Li), xinxinliver@yeah.net (X. Xin), fengqin@shutcm.edu.cn (Q. Feng).
[1] These authors contributed equally to this work.

hepatic APP and Aβ expression, indicating its effectiveness in treating NASH. Furthermore, it inhibited Aβ-induced Cathepsin B lysosomal release, reducing hepatic inflammation.

Conclusion: Danggui-Shaoyao-San has anti-steatohepatitis effects in ameliorating hepatic APP protein expression, reducing hepatic lysosomal CTSB release, and suppressing hepatic NF-κB activation. The study provided a more theoretical basis for the future clinical application of DGSY.

1. Background

Non-alcoholic fatty liver disease (NAFLD), now renamed as metabolic-associated fatty liver disease (MAFLD), engenders metabolic liver stress injuries closely linked to insulin resistance (IR) and genetic predilections [1]. NAFLD encompasses a spectrum of disease states, including non-alcoholic fatty liver (NAFL), non-alcoholic steatohepatitis (NASH), associated liver fibrosis, cirrhosis, and hepatocellular carcinoma [2]. Owing to the rising incidence of obesity and metabolic syndrome, NAFLD is implicated in liver dysfunction and mortality, also manifesting strong associations with the high occurrence of type 2 diabetes and cardiovascular disease. It has now become the most prevalent chronic liver disease in the world. Approximately 25 % of NAFLD cases progress to NASH, serving as an intermediary stage between simple fatty liver to fatty liver fibrosis and liver cirrhosis. Furthermore, at least 25 % of NASH cases escalate into NASH-related liver fibrosis [3]. Effective management and mitigation of NASH development is of paramount importance to decelerate disease progression. However, as of present, the FDA has yet to approve any medication specifically for the treatment of NASH.

DangGui-ShaoYao-San (DGSY), known as Dangguijakyak-san in Korea and Toki-shakuyaku-san in Japan, represents a venerable herbal prescription deeply ingrained within the traditional Chinese medicine (TCM) tradition [4]. Its historical origins can be traced back to the "Jin Kui Yao Lue" (Synopsis of Prescriptions of the Golden Chamber) during the Eastern Han Dynasty, underscoring its enduring legacy [5]. Comprising six herbal components, including, Atractylodes macrocephala Koidz. (Baizhu, Atractylodis macrocephalae rhizoma), Alisma plantago-aquatica Linn. (Zexie, Alismatis Rhizoma), Paeonia lactiflora Pall. (Baishao, Paeoniae Radix Alba), Poria cocos (Schw.) Wolf (Fuling, Poria), Ligusticum chuanxiong Hort. (Chuanxiong, Chuanxiong Rhizoma), and Angelica sinensis (Oliv.) Diels (Danggui, Angelicae Sinensis Radix), this formula's specific herbal ingredient information is presented in Table 1. Furthermore, DGSY has demonstrated its effectiveness in regulating lipid metabolism and ameliorating dyslipidemia [5–9], Alzheimer's disease (AD) [4,10–13], primary dysmenorrhea (PD) [14–17], diabetic nephropathy (DN) [18,19], depression [20–22], etc.

Recent research has thrust DGSY into the spotlight due to its potential significance in combating NASH [23,24]. Nevertheless, the precise molecular processes involved in the hepatoprotective effect of DGSY against NASH remain to be uncovered. This study utilized a high-fat and high-cholesterol (HFHC) induced NASH mouse model, FFA induced hepatocyte cell steatosis model, and network pharmacology methodologies to initially investigate the potential pharmacodynamic mechanisms. Subsequent experimental endeavors were then undertaken to delve into and validate the corresponding pharmacological mechanisms. Our research elucidates a theoretical basis for the clinical application of DGSY, highlighting its molecular actions to aid clinicians in evaluating its potential for NASH treatment protocols. Moreover, the identified pathways and mechanisms offer a foundation for future investigations, enabling researchers to explore NASH treatments across various stages and in conjunction with other therapeutic strategies.

2. Methods

2.1. Preparation of Danggui-Shaoyao-San

DGSY, derived from the original prescription drug composition and dosage detailed in "Jin Kui Yao Lue" comprises six dried crude herbs (Table 1). These medicinal materials were procured from Shanghai Kangqiao Biotechnology Co, Ltd and met the standards stipulated in the Chinese Pharmacopoeia (2020 edition). These herbs underwent a water extraction process, concentrated to a density of 0.48 g crude herb/mL, and subsequently stored at −20 °C until needed. For cell experiments, the DGSY extract was dissolved in a pre-configured medium to create varying concentrations, and then preserved at −20 °C for future use.

Table 1
Composition of DGSY.

Medicinal Chinese Name	Medicinal English Name	Latin Names	Genus	Family
当归	Radix Angelicae Sinensis/Chinese Angelica	*Angellica sinensis (Oliv.)* Diels.	Angelica	Umbelliferac
芍药	Radix Paeoniae Alba/White Peony Root	*Paeonia lactiflora* Pall.	Paeonia	Ranunculaceae
川芎	Rhizoma Chuanxiong/Szechwan Lovage Rhizome	*Ligusticum chuanxiong* Hort.	Ligusticum	Umbelliferae
泽泻	Rhizoma Alismatis/Oriental Waterplantain Rhizome	*Alisma orientalis* (Sam.) Juzep.	Alisma	Alismataceae
茯苓	Poria/Indian Bread	*Poria cocos* (Schw.) Wolf	Poria	Polyporaceae
白术	Rhizoma Atractylodis Macrocephalae/Largehead Atractylodes Rhizome	*Atractylodes macrocephala* Koidz.	Atractylodes	Compositae

3. UHPLC-Q-Orbitrap HRMS

The comprehensive analysis of components within DGSY granules and individual herbal components was conducted using the UHPLC-Q-Orbitrap HRMS technique. In this endeavour, a calibration solution of standard concentration, 1 mg/ml, was employed, and the content of various compounds within the composite formulation was quantified using the peak retention time correlation and single-point external standard quantification method. The experimental setup involved the combined utilization of the Dionex Ultimate 3000 UHPLC system and the Q Exactive mass spectrometer. In terms of chromatographic separation, the chosen conditions encompassed the use of the Acquity UPLC® BEH C18 column, with a mobile phase composed of 0.1 % aqueous formic acid and methanol, achieving separation through gradient elution. On the mass spectrometry front, the utilization of the H-ESI electrospray ionization source was coupled with both positive and negative ion modes, enriched by a two-stage scanning approach that included primary full-scan and data-dependent secondary scans. The analytical scope covered a range of m/z 80 to 1,200, while the collision-induced dissociation energy was varied across three distinct voltage gradients: 20 V, 50 V, and 100 V.

3.1. Animal experimental design

All procedures related to animal experiments received approval from the Animal Experimental Ethics Committee at the Shanghai University of Traditional Chinese Medicine (Permission Number: SZY201710017). Thirty-two male C57BL/6J mice, specific-pathogen-free and aged eight weeks, were randomly sorted into two groups based on body weight (BW): a normal group (n = 8) and a model group (n = 24). All mice were accommodated at the Experimental Animal Center of the Shanghai University of Traditional Chinese Medicine. Following a seven-day adaptation period, the model group received a diet of high-trans fatty acid and high-fructose feed along with fructose-sucrose drinking water. Obeticholic acid (OCA), as an effective agonist of the nuclear receptor FXR, plays a crucial role in regulating bile acids and participating in lipid metabolism, inflammatory response, and the process of fibrosis [25]. The activation of FXR is particularly important for the treatment of NASH, and numerous clinical and animal studies have validated the efficacy of OCA in improving NASH. Therefore, we have chosen it as the positive control drug [26]. The normal group was provided with control feed and regular drinking water and allowed to feed freely. The establishment of a non-alcoholic mouse steatohepatitis model was achieved after 25 weeks of this feeding regimen [27]. Subsequently, mice in the model group were divided into three further groups: HFHC, DGSY, and OCA (n = 8 per group). The mice were administered DGSY and OCA via gavage at doses of 25.8 g/kg BW and 10 mg/kg BW, respectively, every 24 h. The control group received drinking water. Throughout the experiment, animals had unrestricted access to food and water. After four weeks, the 32 mice were anesthetized and euthanized, and their livers were collected for subsequent study.

The original prescription from "Jin Kui Yao Lue" records a daily dosage of raw medicine for adults as 129 g, consisting of Atractylodes macrocephala Koidz. 12 g, Alisma plantago-aquatica Linn. 24 g, Paeonia lactiflora Pall. 48 g, Poria cocos (Schw.) Wolf 12 g, Ligusticum chuanxiong Hort. 24 g, and Angelica sinensis (Oliv.) Diels 9 g. The dosage concentration for mice, adjusted for body surface area and previous preliminary studies [28], yields a final concentration of 25.8 g/kg for each mouse per day [29].

3.2. Cell viability assay

Cells were uniformly seeded in 96-well plates at a cell density of 8000 pcs/well, and after 24 h of cell adhesion, the medium was replaced with DMEM medium containing 0, 0.5, 1, 2, 3, and 4 mg/ml DGSY for 24 h, with 6 wells in each group. After 24 h, discard the supernatant and add medium containing 10 % CCK8 reagent and incubate in a 37 °C cell culture incubator. At 0.5 h, 1 h, 2 h, the 96-well plates were placed into a multifunction microplate reader to read the absorbance value at 450 nm for statistical analysis.

3.3. Cell culture and treatment

Human hepatocyte L02 cell line was obtained from the cell bank of the Shanghai Institute of Cell Biology, Chinese Academy of Sciences. Cells were cultured in DMEM (No. 11965092, Gibco, Thermo Fisher) supplemented with 10 % FBS (No. 10099-141C, Gibco, Thermo Fisher) with 1 % penicillin–streptomycin (No. 30-002-Cia, Corning Cellgro) at 37 °C in an incubator with 5 % CO^2. The configuration method of FFA (free fat acid) was to dissolve 0.0513 g of palmitic acid (No. P5585, Sigma) in 10 ml isopropanol, 1 ml of which was taken after filtration and 16 μl sterile oleic acid (No. 01383, Sigma) was added to obtain FFA solution with a concentration of 1 mM. The results of CCK8 showed that DGSY extract was not cytotoxic between 0 and 4 mg/ml. Therefore, intermediate doses of 1 mg/ml and 2 mg/ml were chosen as the optimal doses for subsequent experiments (Fig. S1). Cells are seeded in 12-well plates at a density of 3.5×10^4 pcs/well. After 24 h, the cells were divided into 4 groups with 4 complex wells each, and the four groups were control group (Con), model group (FFA, 0.2 mM FFA), DGSY low-dose group (DGSY-L, 0.2 mM FFA and 1 mg/ml DGSY), DGSY high-dose group (DGSY-H, 0.2 mM FFA and 2 mg/ml DGSY) for 24 h. Cells were collected for subsequent testing.

3.4. Animal sample collection

At the end of the 29th week, the mice were fasted for 12 h and anesthetized with 2 % sodium pentobarbital intraperitoneal injection at a dose of 3 mL/kg (BW). 1 mL of blood was collected from each mouse. A part of the liver tissue was extracted from the same lobe and location of each mouse and fixed in a 10 % neutral buffered formalin solution. A part of the tissue was taken out and wrapped in ornithine carbamoyltransferase (OCT) gel, and then quickly frozen in liquid nitrogen for sectioning. The remaining liver tissue was

placed in a 2 mL Eppendorf tube and stored in the refrigerator for later use at −80 °C.

3.5. Biochemical analysis

The activity of serum ALT and AST was measured using commercial kits (Lot number 20180628, Nanjing Jiancheng Institute of Biotechnology, Nanjing. TG content in liver and hepatocyte samples was measured using a kit (Lot number 2018080029, Dong'ou Diagnostic Products Co. Ltd, Zhejiang, China). Fasting blood glucose (FBG) was measured with a blood glucose meter (Roche diagnostic GmbH, Germany). Fasting insulin (FINS) level was measured using the mouse insulin ELISA (lot number: 90080, ALPCO, America). And the homeostasis model assessment of basal insulin resistance (HOMA-IR) was calculated using the formula FBG (mM) $\times$ FINS (μU/mL)/22.5.

3.6. Hematoxylin and eosin (H&E) staining

Liver tissue was fixed in 10 % neutral buffered formalin solution and sectioned at a thickness of 10 μm. The sections were stained using an H&E staining kit (lot number 20180530, Nanjing Jiancheng Bioengineering). Images were analyzed using a light microscope (Olym-pus BX40, Tokyo, Japan).

3.7. Oil red O staining

Liver tissue was embedded in OCT medium, fixed in liquid nitrogen, and sectioned at a thickness of 4 μm at −20 °C. The sections were stained using an Oil red O staining kit (lot number 20180528, Nanjing Jiancheng Bioengineering). Images were analyzed using a light microscope (Olym-pus BX40, Tokyo, Japan). The procedure for oil red O staining of cells are as follows: The cells were rinsed with PBS for 2–3 times, fixed with 10 % formaldehyde for 30 min at room temperature, the oil red O stock solution and diluent were prepared according to the ratio of 5:2 and filtered, then formaldehyde was discarded, 400–500 μl oil red dyeing solution was added to each well to dye for 30 min at room temperature, 400 μl 60 % isopropanol was rinsed to remove excess dye, 200 μl counterstaining solution was added to each well for 10 s, and the cells were rinsed with PBS and photographed under a microscope.

3.8. Screening of active compounds and target screening in Danggui-Shaoyao-San

Compounds with good pharmacokinetics are filtered according to the attributes of the ADME system (absorption, distribution, metabolism and excretion), whose parameters includes oral bioavailability (OB) and drug-likeness (DL), Active compounds of DGSY were identified based on and UHPLC-Q-Orbitrap HRMS and TCMSID [30]. NASH and DGSY-related genes were obtained using the GeneCards (https://www.genecards.org/) [31] and SwissTargetPrediction [32]. After merging NASH and DGSY-related targets, overlapping targets were recognized as candidate targets. Then, a Venn diagram was established by importing the gene ID of DGSY and NASH-related targets to the STRING database (https://string-db.org/) [33].

3.9. Protein-protein interaction network construction

Based on candidate targets, a protein-protein interaction (PPI) network was established by importing the gene ID of the candidate targets to the STRING database. Cytoscape 3.6.1 was used to visualize the PPI network. Cytoscape's CytoHubba was used to perform weight analysis and created a network of the key protein interactions.

3.10. Reverse transcription polymerase chain reaction

Total RNA was extracted from hepatic tissue using trizol reagent. Extracted RNA was transcribed into cDNA by employing a reverse transcription kit (RNA extraction, Sangon Biotech [Shanghai] Co., Ltd. B511321; RNA reverse transcription, BioRad, 1708890). Nucleotide sequences of the PCR primers are shown in Table S1. The RT-PCR procedure was performed as follows: pre-denaturation at 95 °C for 30 s, denaturation at 95 °C for 5 s, annealing at 60 °C for 32 s, and elongation at 95 °C for 15 s; repeated for 50 cycles, following the manufacturer's instructions.

3.11. Western blot analysis

The total proteins from liver tissues or hepatocytes were extracted using RIPA lysis buffer, and protease and phosphatase inhibitors. The concentration of protein extracts was quantified using the BCA Protein Assay kit (Beyotime Institute of Biotechnology, Jiangsu, China). The proteins were separated by sodium dodecyl sulfate-polyacrylamide gel electrophoresis (SDS-PAGE) and blotted to poly-vinylidene fluoride (PVDF) membranes through the semi-wet electrophoretic transfer method. The membranes were blocked with 5 % bovine serum albumin (BSA; Biotech well, WH1057-1) for 1 h at 37 °C, the blots were incubated with primary antibodies against APP (Abcam, ab32136, 1:1000), Aβ (Abcam, 201060, 1:1000), p65 (CST 8242, 1:1000), p-p65 (CST, 3033, 1:1000), TNF-α (Abcam, ab183218, 1:1000) and GAPDH (Abcam, ab8245, 1:1000) at 4 °C overnight. Then the membranes were incubated with relevant HRP-conjugated secondary antibodies. The expression level of the proteins was detected using ECL Imager.

3.12. Immunofluorescence staining

The sections of liver tissues were fixated and blocked routinely, followed by incubation with primary antibodies of lysosomal associated membrane protein-1 (LAMP-1) (Santa Cruz Biotechnology, 1D4B, 1:250) and CTSB (Abcam, ab32136, 1:250) overnight at 4 °C. The sections were incubated with Alexa Fluor 488 secondary antibodies (Abcam, AB150073, 1:250) and Alexa Fluor 647 (Abcam, ab150155, 1:250) at room temperature away from light. Then, the sections were fixed in 4′,6-diamidino-2-phenylindole (DAPI, Abcam,

Fig. 1. Identification of Active Compounds Utilizing UHPLC-Q-Orbitrap HRMS. (A). Total ion chromatogram of the DGSY granule solution obtained through UHPLC-Q-Orbitrap HRMS, showcasing the comprehensive chemical composition of the formulation. (B). Quantitative representation of the compounds found in the DGSY granule solution.

ab104139) at a dilution of 2.5 μg/mL for 10 min to visualize the nuclei. Fluorescent antigen distribution was observed using a fluorescence microscope and analyzed with Image-Pro Plus 7.0. For the cell experiment, L02 were seeded into 24-well plates with microscope coverslips and treated as indicated. Cells were immunostained with anti-LAMP and anti-CTSB primary antibodies, and secondary antibodies were conjugated with AlexaFluor 488, and Alexa Fluor 647 as described above, and then examined with a laser confocal scanning microscope.

3.13. Statistical analysis

Statistical analysis was performed using GraphPad Prism version 8.0 (GraphPad Software, La Jolla, CA). Data were expressed as mean ± standard deviation. Data were analyzed using test-test or one-way ANOVA analysis of variance and least significant difference test, and $P < 0.05$ was considered statistically significant.

4. Results

4.1. Identification of active compounds utilizing UHPLC-Q-Orbitrap HRMS

A total of 34 compounds from the DGSY were meticulously examined employing UHPLC-Q-Orbitrap HRMS. Utilizing concurrent positive and negative ion scanning modes, each compound underwent rigorous confirmation via reference standard comparisons. The comprehensive total ion chromatogram of the DGSY granule solution is displayed in Fig. 1A, while the outcomes of the component identification are compiled in Table 2. Furthermore, Fig. 1B depicts the quantities of the compounds in the formulation, with the top ten DGSY components listed as follows: Paeoniflorin, Albiflorin, Catechin, Gallic Acid, Atractylenolide III, Palmitic Acid, Ferulic Acid, Caffeic Acid, p-Hydroxybenzoic acid, and Neochlorogenic Acid.

4.2. Danggui-Shaoyao-San reduces body and liver weight, and improves lipid and glucose metabolism in mice

Upon conclusion of a 29-week dietary regimen (Fig. 2A), the liver and body dimensions in the mouse model group had markedly increased, but these were attenuated following treatment with DGSY or OCA, as depicted in Fig. 2B.

Table 2
Component identification of DGSY utilizing UHPLC-Q-Orbitrap HRMS.

no.	Compound	Molecular formula	Calculated Mass/Da	t_R/min	Ion mode	Concentration (ug/ml)
1	Gallic Acid	$C_7H_6O_5$	169.013	2.02	[M − H]-	34.53614757
2	3,4-Dihydroxybenzoic Acid	$C_7H_6O_4$	153.018	4.14	[M − H]-	0.473005991
3	3,4-Dihydroxybenzaldehyde	$C_7H_6O_3$	137.023	6.40	[M − H]-	0.122637315
4	Oxypaeoniflorin	$C_{23}H_{28}O_{12}$	495.150	9.91	[M − H]-	4.534793619
5	Ferulic Acid	$C_{10}H_{10}O_4$	195.065	14.96	[M+H]+	11.18229716
6	Neochlorogenic Acid	$C_{16}H_{18}O_9$	353.087	6.52	[M − H]-	8.325662156
7	Caffeic Acid	$C_9H_8O_4$	181.050	9.68	[M+H]+	9.196702908
8	Epicatechin Gallate	$C_{15}H_{14}O_6$	289.071	12.02	[M − H]-	0.245790891
9	Ligustilide	$C_{12}H_{14}O_2$	191.107	33.23	[M+H]+	0.562726702
10	Albiflorin	$C_{23}H_{28}O_{11}$	525.160	12.58	[M-COOH]-	173.2071143
11	Naringenin	$C_{15}H_{12}O_5$	271.060	24.72	[M − H]-	0.023543553
12	p-Hydroxybenzoic Acid	$C_7H_6O_3$	139.039	8.46	[M+H]+	8.416308273
13	Cryptochlorogenic Acid	$C_{16}H_{18}O_9$	353.087	10.66	[M − H]-	7.735148545
14	Cynarin	$C_{25}H_{24}O_{12}$	515.118	12.37	[M − H]-	4.193867944
15	3-n-Butylphthalide	$C_{12}H_{14}O_2$	191.107	30.59	[M+H]+	0.050149506
16	Levistilide A	$C_{24}H_{28}O_4$	381.206	40.11	[M+H]+	0.035478371
17	Palmitic Acid	$C_{16}H_{32}O_2$	279.229	41.11	[M+Na]+	11.52016593
18	Ethyl Ferulate	$C_{12}H_{14}O_4$	223.096	27.53	[M+H]+	0.019845861
19	Senkyunolide A	C12H16O2	193.122	29.97	[M+H]+	6.419633093
20	Senkyunolide A	$C_{12}H_{16}O_4$	225.112	20.12	[M+Na]+	3.270243104
21	3-Butylidenephthalide	C12H12O2	211.073	33.89	[M+Na]+	0.00305546
22	Paeonol	C9H10O3	165.055	22.86	[M − H]-	3.998386865
23	Ligustrazine	C8H12N2	137.107	9.70	[M+H]+	0.0234
24	Alisol A	$C_{30}H_{50}O_5$	513.355	41.20	[M+Na]$^+$	4.469833494
25	Paeoniflorin	C23H28O11	525.160	14.20	[M + COOH]-	244.9661291
26	Chlorogenic Acid	$C_{16}H_{18}O_9$	353.087	9.68	[M − H]-	8.046139198
27	Benzoylpaeoniflorin	C5H8O2	145.050	41.20	[M + COOH]-	4.575863533
28	Pachymic Acid	C33H52O5	529.389	41.71	[M+H]+	0.049347508
29	Catechin	C15H14O6	289.071	8.47	[M − H]-	79.67862317
30	Alisol B	C30H48O4	473.363	41.20	[M+H]+	4.623071809
31	23-Acetyl alisol C	C32H48O6	529.352	37.36	[M+H]+	0.497822533
32	Atractylenolide I	C15H18O2	231.138	38.91	[M+H]+	0.028683444
33	Atractylenolide II	C15H20O2	233.154	36.35	[M+H]+	0.38111407
34	Atractylenolide III	C15H20O3	271.130	34.25	[M+Na]	16.36446398
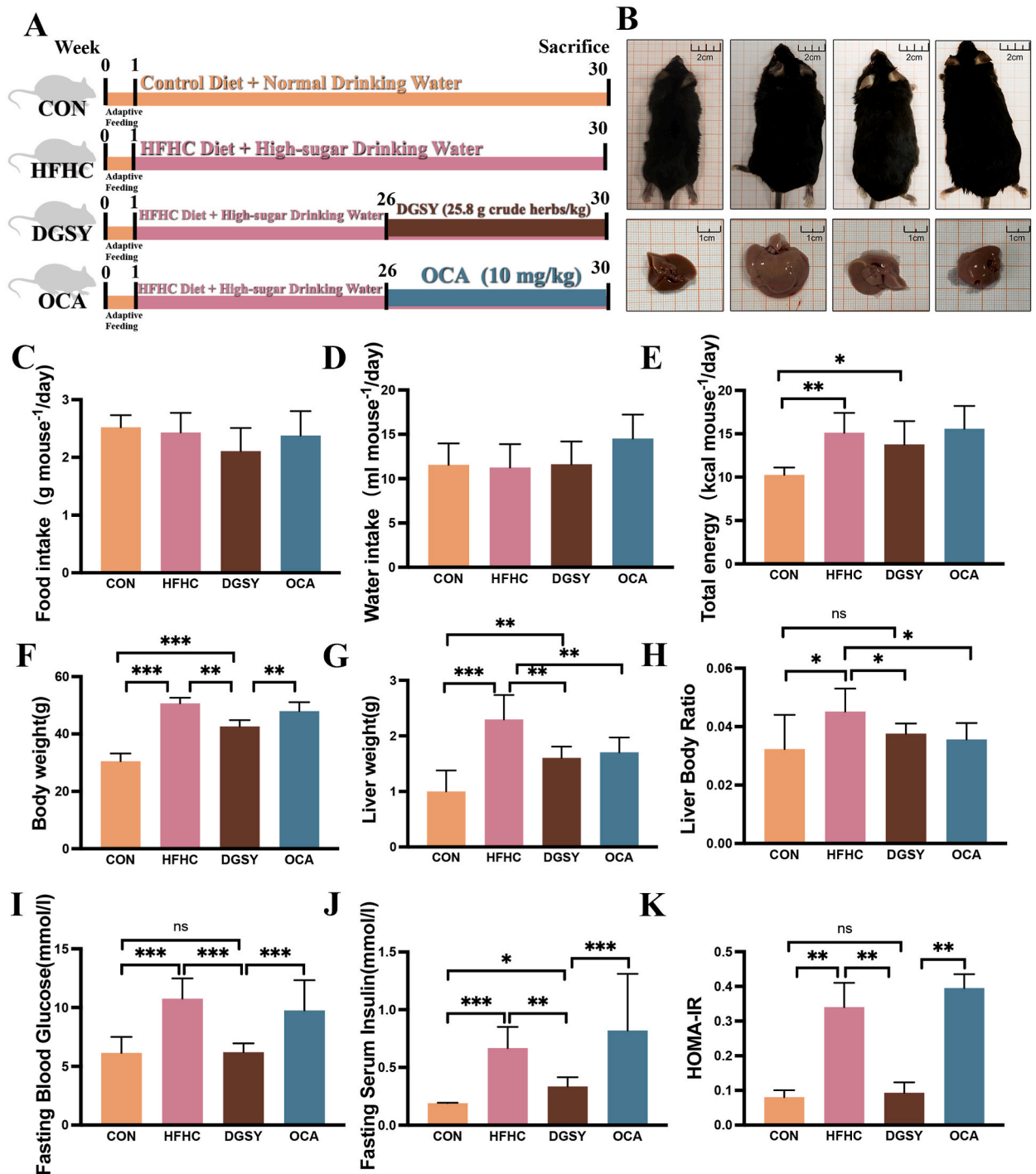
Fig. 2. DGSY lessens body and liver weight and enhances lipid and glucose metabolism in mice. (A). Photographic depiction of mice body and liver. (B). Mean food intake. (C). Water consumption. (D). Total caloric intake. (E). Body weight. (F). Liver weight. (G). Body-to-liver weight ratio. (H). Fasting Blood Glucose levels. (I). Fasting Serum Insulin levels. (J). HOMA-IR values. Significant variances are designated as: *$P < 0.05$, **$P < 0.01$, ***$P < 0.001$, Control Group (CON); Model Group (HFHC: high-fat/carbohydrate/cholesterol/choline diet); Danggui-Shaoyao-San Group (DGSY).

Notwithstanding uniform food and water intake across the four cohorts post the 29-week mark, a significant elevation in total energy was documented in the HFHC group relative to the control group at this stage (Fig. 2C, D, 2E). Subsequent to DGSY therapy, a progressive decline in total energy was recorded, although it remained higher than that of the control group on a standard diet (Fig. 2E).
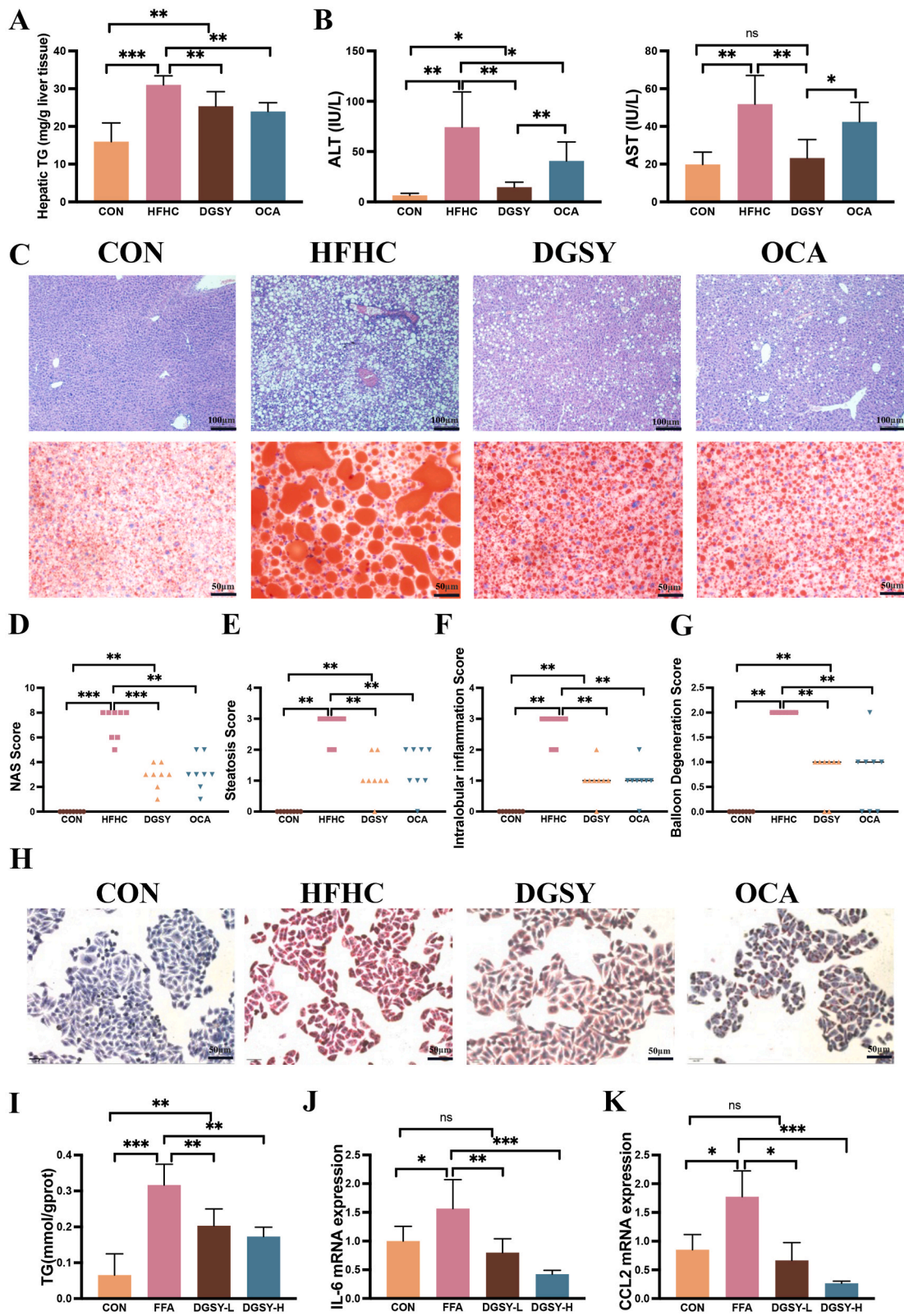
(caption on next page)

Fig. 3. DGSY mitigates hepatic steatosis and inflammatory damage both *in vivo* and *in vitro*. (A). Variations in hepatic triglycerides (TG) content across different mice groups. (B). Changes in hepatic alanine aminotransferase (ALT) and aspartate aminotransferase (AST) content across the groups. (C). Liver tissue stained with H&E (hematoxylin-eosin); Oil Red O staining. (D). Alterations in NAS score. (E). Hepatocyte steatosis score. (F). Intralobular inflammation score. (G). Hepatocyte ballooning score across the groups. (H). Oil Red O staining illustrating lipid accumulation in L02 cells. (I). TG content in L02 cells. (J). mRNA expression level of IL-6. (K). mRNA expression level of CCL2. *$P < 0.05$, **$P < 0.01$, ***$P < 0.001$.

The body and liver masses of mice subjected to the HFHC diet were appreciably greater than those nourished with a matched normal diet (Fig. 2F and G). Treatment with DGSY or OCA resulted in a substantial reduction in both body and liver weights, yet these weights remained above those observed in the control group.

The body-to-liver weight ratio in the HFHC cluster exceeded that of the control group (Fig. 2H), and it substantially decreased following DGSY administration, though it remained higher than that of the control group. Despite the absence of a difference in body weights between the HFHC and OCA groups, hepatic masses diminished remarkably (Fig. 2F), accompanied by a reduction in the body-to-liver weight ratio following medication administration (Fig. 2H).

The HFHC group exhibited elevated FBG, FINS, and HOMA-IR compared to the control group ($P < 0.01$). DGSY ameliorated the HFHC diet-induced hyperglycemia (Fig. 2I, J, 2K), although OCA treatment did not yield a notable improvement in glucose metabolism (Fig. 2I, J, 2K). In terms of FBG and HOMA-IR, the DGSY treatment restored levels to those comparable to the control group. However, for FINS, levels after DGSY treatment remained elevated above those of the control group.

4.3. Danggui-Shaoyao-San mitigates hepatic steatosis and inflammation in vivo and in vitro

At 29 weeks, the serum activity of ALT and AST and the content of TG in the HFHC group mice were significantly higher than those in the control group mice, and these biological function-related indicators are significantly reduced after medication (Fig. 3A and B). The administration of DGSY effectively lowered the levels of TG and AST, yet they did not return to the levels observed in the control group. However, the AST levels were normalized to the control group's levels after DGSY treatment.

H&E staining of the liver tissue showed that hepatic steatosis affected the entire liver lobule, with substantial inflammatory cell infiltration and scattered necrosis. Inflammation and different degrees of balloon-like degeneration were seen in HFHC mice at 29
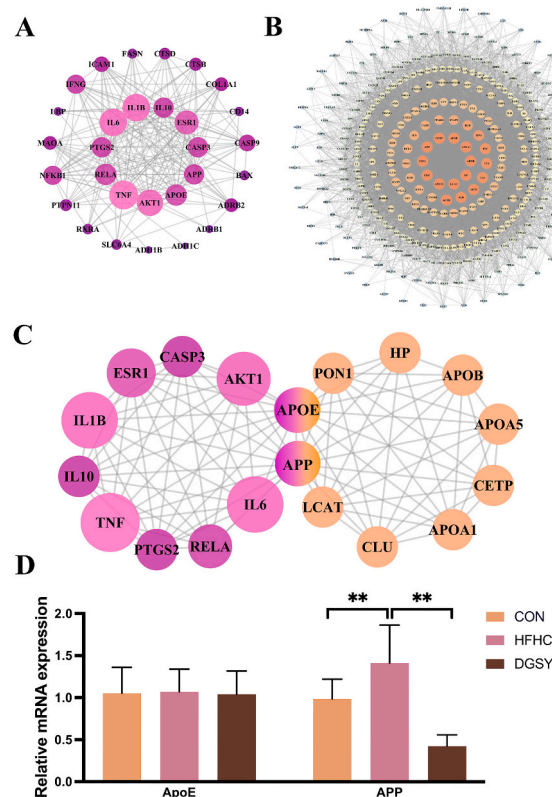

Fig. 4. Network pharmacology indicates that amyloid precursor protein (APP) could be a potential drug target for DGSY. (A). Intersection of target points of the monomer and the disease. (B). Protein-protein interaction network showcasing dense interactions. (C). Utilization of CytoHubba, a plugin in Cytoscape, to conduct weight analysis and create a network of the top ten protein interactions. (D). mRNA expression level of the selected 9 genes, **$P < 0.01$.

weeks. After DGSY treatment, the fatty degeneration of the liver tissue significantly improved. Balloon-like degeneration and inflammation damage of hepatocytes were rare or absent (Fig. 3C). Similarly, Oil red O staining of the liver tissues in the HFHC group showed that the hepatocytes were obviously enlarged and round and had more lipid droplets stained with oil red. Compared with the liver tissue of the HFHC group, liver tissues of the DGSY group had fewer red lipid droplets (Fig. 3C). Additionally, steatosis, ballooning degeneration, lobular inflammation, and NAFLD activity scores (NAS Score) in the HFHC group were higher than those in the control group. The four scores significantly decreased after DGSY treatment ($P < 0.01$), and there was a significant difference between the DGSY group and OCA group in steatosis, ballooning degeneration, lobular inflammation score. Although OCA also improved inflammation damage and steatosis, its therapeutic efficacy was far less than that of DGSY (Fig. 3D, E, 3F, 3G).

Since hepatocytes are the main cell type of liver structure, they are the main cells of fatty acid-induced lipotoxicity, we then investigated the effects of DGSY on hepatocytes under steatosis. The CCK-8 test results showed that DGSY had no cytotoxic effect on L02 cells within 4 mg/ml (Fig. S1), so we selected two intermediate doses of 1 and 2 mg/ml for subsequent experiments. We treated L02 cells with FFA to induce a model of steteaosis. The results of oil red O staining analysis showed increased lipid accumulation in hepatocytes with FFA added compared to control cells. This increase was reduced by DGSY at concentrations of 1 and 2 mg/ml (Fig. 3H). Similarly, TG levels were also significantly elevated in FFA-induced L02 cells and was improved after 1 and 2 mg/ml DGSY administration (Fig. 3I). However, the TG content did not return to the baseline levels of the control group after treatment with DGSY. Furthermore, DGSY significantly attenuated FFA-induced up-regulation of inflammatory genes IL-6, CCL2 (Fig. 3J and K), with the mRNA expression levels of these genes returning to those of the control group post-treatment.

4.4. Potential pharmacological target of Danggui-Shaoyao-San for NASH: A focus on APP via multiple network pharmacology analysises

Among the 34 constituents identified through UHPLC-Q-Orbitrap HRMS analysis in the DGSY standard decoction, we utilized SwissTargetPrediction identified a total of 194 predictive proteins (Additional file 3: Table S2). SwissTargetPrediction operates on the principles of assessing the structural similarity between known compounds, both in two-dimensional and three-dimensional contexts, to predict the potential targets of compounds. We curated 1643 NASH-associated protein from GeneCards (Additional file 4: Table S3). Employing a Venn diagram analysis with the 1643 disease proteins and the 194 active compound related proteins, we identified 30 overlapping proteins (Additional file 5: Table S4). To gain a comprehensive understanding of how the DGSY standard decoction may treat NASH, we imported the gene names of these 30 NASH proteins into the STRING database. Subsequently, using Cytoscape and considering protein degree, we constructed a protein-protein interaction (PPI) network (Fig. 4A). The top 10 core proteins were
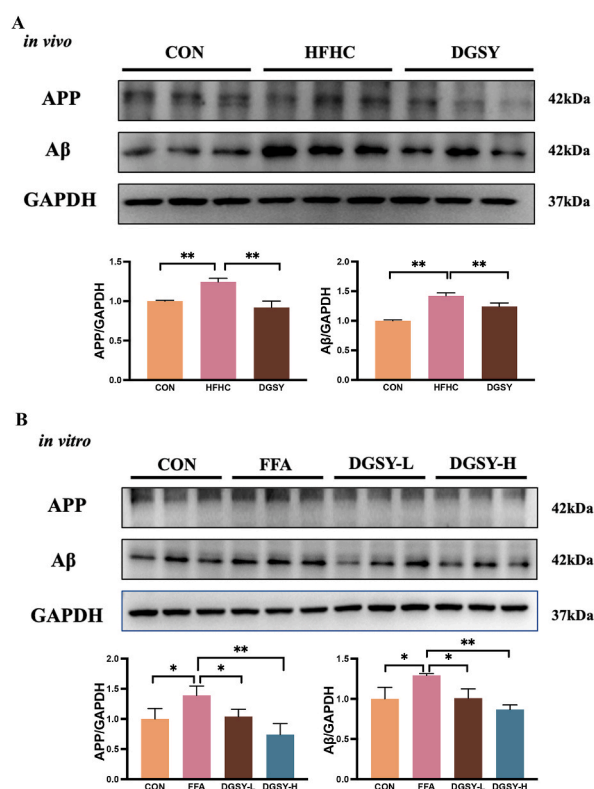
Fig. 5. DGSY markedly reduces hepatic APP protein and its metabolite, amyloid beta (Aβ), both *in vivo* and *in vitro*. (A). APP and Aβ protein levels in mice. (B). APP and Aβ protein levels in L02, with GADPH used as a loading control. n = 3, *$P < 0.05$, **$P < 0.01$. Full-length blots are presented in Additional file 8.

identified based on their degree value, namely Tumor Necrosis Factor (TNF), Interleukin 1 Beta (IL1B), Interleukin 6 (IL6), AKT Serine/ Threonine Kinase 1 (AKT1), Estrogen Receptor 1 (ESR1), Apolipoprotein E (APOE), Nuclear Factor Kappa B Subunit RelA (RELA), Amyloid Precursor Protein (APP), Interleukin 10 (IL10), Prostaglandin-Endoperoxide Synthase 2 (PTGS2).

The aforementioned network pharmacology screening is rooted in SwissTargetPrediction, which relies on the structural similarity of known compounds in both two and three dimensions. As part of our ongoing research, we plan to conduct another network pharmacology analysis using the TCMSP database to further refine our results. The TCMSID database is a widely utilized resource, serving as a comprehensive search platform with literature-based evidence on traditional Chinese medicine ingredients and target information, with a specific focus on herbal component targets (+). We identified 1781 genes associated with DGSY in TCMID (Additional file 6: Table S5). As shown in Table S6, we found 362 protein that overlapped out of the 1643 NASH-associated protein. A PPI network was subsequently constructed, integrating the shared 362 protein targets (Fig. 4B). Among the 362 proteins, the top ten differentially expressed proteins were identified through degree analysis in Cytoscape. These proteins include cholesteryl ester transfer protein (CETP), apolipoprotein A1 (ApoA1), apolipoprotein A5 (ApoA5), apolipoprotein B (ApoB), Phosphatidylcholine-sterol acyl-transferase (LCAT), paraoxonase-1 (PON1), ApoE, APP, clusterin (CLU), and haptoglobin (Hp).

APOE and APP emerged as the top 10 candidates from our previous target prediction analyses, which encompassed both structural prediction and literature evidence (Fig. 4C). Subsequently, we conducted an analysis of their transcription levels using PCR. Notably, it is important to highlight that only the transcription level of APP exhibited a significant increase following induction by a HFHC diet ($P < 0.05$), which was subsequently reversed after DGSY administration ($P < 0.01$), as depicted in Fig. 4D. In contrast, the mRNA expression of APOE remained unchanged, which was inconsistent with the initial prediction. (Fig. 4D).

4.5. Danggui-Shaoyao-San effectively suppresses hepatic APP protein and its metabolite aβ expression

Following the network pharmacological screen, APP emerged as a prospective therapeutic target of DGSY for NASH amelioration. APP is best known as the precursor molecule whose proteolysis generates amyloid beta (Aβ) [34]. Importantly, APP and its hydrolytic product Aβ may be closely associated with the development of various metabolic disorders, such as obesity, type 2 diabetes (T2DM), and NAFLD [35–37]. Inhibiting the expression of APP can improve NAFLD [34]. It is worth emphasizing that multiple studies have shown that DGSY can improve AD through its effects on APP.

We utilized Western blotting to ascertain the levels of APP protein expression. The hepatic expression of the APP protein in the HFHC group at the 29-week mark was found to be considerably elevated as compared to the control group. Importantly, this elevated APP protein expression was markedly reduced following the administration of DGSY (Fig. 5A, $P < 0.01$).

APP undergoes cleavage by secretase, resulting in the production of Aβ. Hence, Western blotting was further employed to examine
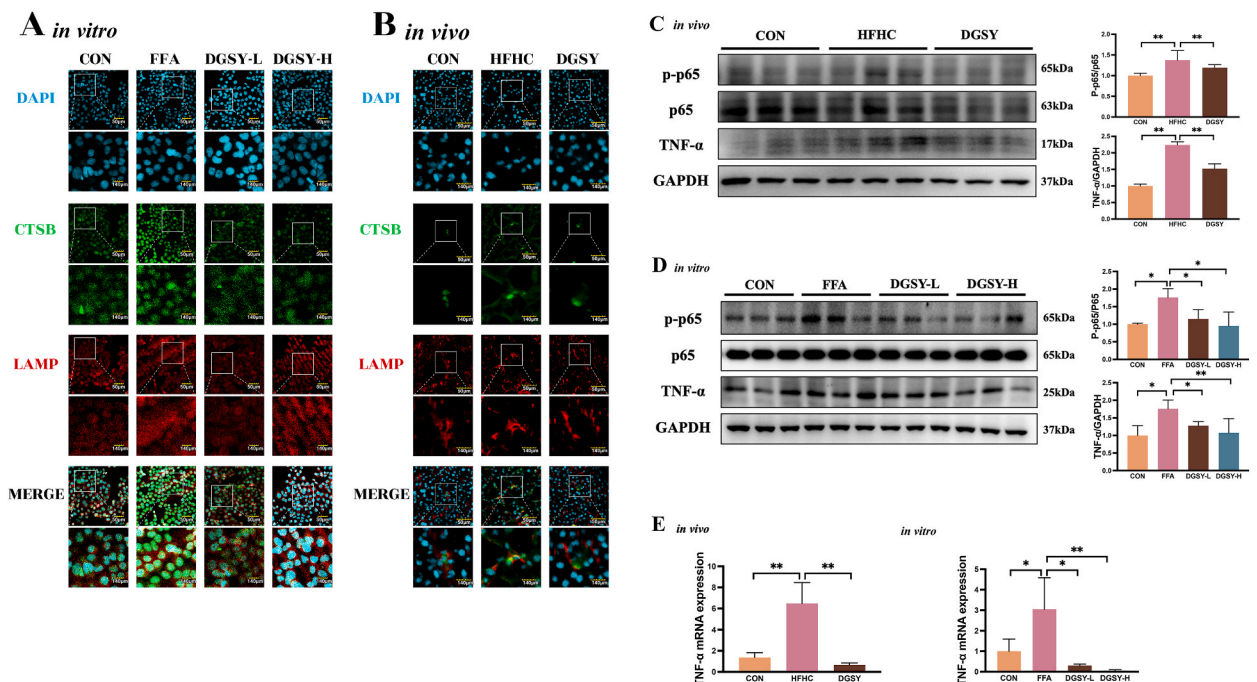
Fig. 6. DGSY significantly curtails Aβ-induced lysosomal release of CTSB (cathepsin B) in hepatocytes, hinders NF-κB pathway activation, and mitigates liver inflammatory damage *in vivo* and *in vitro*. (A–B). Confocal microscopy images of liver tissue (A) and L02 cells (B) stained with anti-CTSB (green) or anti-LAMP (red); nuclei stained with DAPI (blue). (C–D). Phosphorylation levels of p65 and protein levels of TNF-α in liver tissue (C) and L02 cells (D). (E). Transcription levels of TNF-α in liver tissue and L02. *$P < 0.05$, **$P < 0.01$. Full-length blots are presented in Additional file 8.

the hepatic Aβ protein expression levels. The HFHC group demonstrated a significant increase in Aβ protein expression compared to the control group, which was notably attenuated following DGSY administration (Fig. 5A, $P < 0.01$).

In addition, we explored the impact of DGSY on the protein expression of APP and Aβ in the L02 cell lines. Concordant with expectations, FFA induction led to an upregulation of APP and Aβ protein expression levels. This upregulation, however, was reversed by DGSY within the L02 cell lines (Fig. 5B).

Collectively, these findings suggest that DGSY significantly reduces the expression of APP and its metabolite Aβ, demonstrating its effectiveness both *in vivo* and *in vitro*.

4.6. Danggui-Shaoyao-San effectively thwarts aβ-induced cathepsin B lysosomal release in hepatocytes, mitigating hepatic inflammatory damage

In our study, APP and its derivative, Aβ, hold a pivotal role. Previous research has established that Aβ triggers the release of Cathepsin B (CTSB) from lysosomes. CTSB, classified as a cysteine protease, carries out essential protein degradation functions within the endolysosomal system via endocytosis or phagocytosis. Increased CTSB release can lead to hepatic lipid deposition, infiltration of inflammatory cells, and even the development of liver fibrosis [38–42].

Our study implemented immunofluorescence to confirm the pronounced increase in CTSB expression and its colocalization with LAMP-1 in both the liver of HFHC mice and L02 cells. Observations from the fluorescent images revealed a diffused pattern of hepatocytes in the model mice group. However, post-DGSY administration, the immunofluorescence exhibited a punctate distribution of CTSB, aligning with the pre-medication localization of lysosomes (Fig. 6A,B) (see Fig. 7).

Feldstein et al. [43] found that stimulating liver cells with FFA leads to lysosomal damage in liver cells, promoting the release of CTSB from lysosomes into the cytoplasm, thereby increasing the activation of NF-κB. This upregulates the mRNA and protein expression of downstream inflammatory factor TNF-α, ultimately resulting in liver cell damage. During our investigation, we observed that DGSY demonstrates a remarkable ability to alleviate inflammation, both *in vivo* and *in vitro*. Given these findings, our research now places a significant focus on APP/CTSB/NF-κB-related inflammation.

Subsequently, Western Blot was further performed to identify the expression levels of NF-κB p65 and TNF-α proteins. The HFHC or FFA-induced phosphorylation of NF-κB p65 was noted to be reduced by DGSY treatment ($P < 0.05$, Fig. 6C and D). Concurrently, the model group exhibited a marked increase in TNF-α levels as compared to the control group. Notably, the enhanced transcription level of TNF-α in the model group was tempered following DGSY treatment ($P < 0.01$, Fig. 6E).

Taken together, these findings suggest that DGSY is capable of inhibiting the lysosomal release of CTSB, facilitated by the APP metabolite Aβ in hepatocytes. Consequently, this inhibits the activation of the NF-κB and the release of TNF-α.

5. Discussion

This study demonstrated that DGSY could ameliorate NASH. Intriguingly, DGSY exhibited potent efficacy in mitigating inflammation damage. Through bioinformatics analysis using multiple databases, APP emerged as a potential key molecular target that
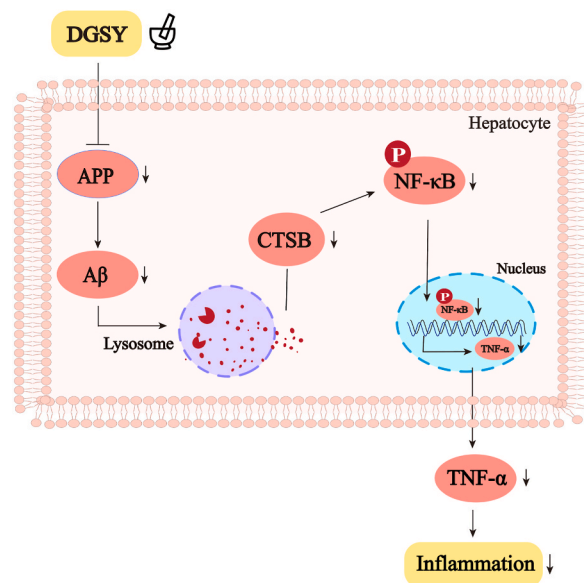
Fig. 7. Underlying mechanism of DGSY in the treatment of NASH. It has been shown that DGSY effectively curtails the expression of hepatic APP, a crucial target potentially implicated in NASH-related processes. This results in the downregulation of Aβ-induced lysosomal release of CTSB, thereby inhibiting the activation of the NF-κB pathway.

mediates the anti-NASH effect of DGSY. DGSY suppressed the release of CTSB from lysosomes in hepatocytes, which was instigated by the metabolite of APP, Aβ. This suppression consequently inhibited the activation of the NF-κB signaling pathway, along with the transcription and release of TNF-α, thereby attenuating hepatic inflammatory damage. Collectively, these findings provided further evidence that DGSY might improve liver inflammation damage in HFHC induced NASH by inhibiting hepatic APP protein expression, reducing hepatic lysosomal CTSB release, and suppressing hepatic NF-κB activation.

Prior experimental results indicated that DGSY exhibited a potent therapeutic effect on NAFLD [23]. DGSY may ameliorate metabolic fructose diet-induced syndrome, with its therapeutic effect potentially linked to gut microbiota modulation, lipid homeostasis improvement, and dysglycemia mitigation [7]. In this study, we discerned that DGSY effectively enhanced glycolipid metabolism, mitigated liver inflammation and steatosis in NASH mice, and improved FFA-induced lipid deposition in L02 cells. However, the specific mechanism through which DGSY ameliorates NASH remains elusive. We employed a multi-step approach to identify potential pharmacological targets for DGSY in the context of NASH. Remarkably, among these core proteins, APP and APOE emerged as compelling candidates. Network pharmacology predicts potential drug targets using bioinformatics methods, but these predictions need experimental validation. To validate their significance, we performed transcriptional analysis using PCR. Significantly, APP demonstrated a notable increase in transcription levels following induction by a HFHC diet. Interestingly, this increase in APP transcription was subsequently reversed upon DGSY administration. Whereas APOE showed no change at the mRNA level. The validation of APP as a target of DGSY is reinforced by multiple studies demonstrating the interaction between DGSY and APP in AD therapy. APP expression exhibits a positive correlation with obesity and exerts a detrimental impact on NAFLD. An et al. [44] discovered that adipo-APP transgenic mice developed hepatic steatosis with elevated liver TG levels. In contrast, APP knockdown mice showed a significant reduction in liver steatosis. Consequently, we hypothesized that the mechanism of DGSY in treating NASH might be connected with APP and its downstream signaling pathways. Our results verified that DGSY indeed downregulated the expression of APP and its metabolite Aβ *in vivo* and *in vitro*. Aβ, produced by APP through sequential cleavage by β-secretase and γ-secretase complex [45], when phagocytosed by microglial lysosomes, leads to lysosomal swelling and potential dysfunction. Subsequently, CTSB is released from lysosomes into the cytoplasm, activating NF-κB and inducing TNF-α expression [46].

CTSB is a cysteine protease found in the lysosome and is involved in the pathological process of various diseases [47]. The release of CTSB from the lysosome can induce lysosomal permeabilization, leading to cellular inflammation, stress, and apoptosis. A clinical study observed the translocation of CTSB from lysosomes to the cytoplasm in human liver biopsies from patients with NAFLD, indicating that hepatic CTSB is involved in lysosomal disruption. Moreover, the lysosomes of hepatocytes, when stimulated by free fatty acids, can induce TNF-α expression, and the release of pro-inflammatory factors is CTSB-dependent [48]. In our study, we discovered that an increase in Aβ in liver tissue might lead to the release of CTSB from lysosomes. After administering DGSY, we found a significant reduction in CTSB within lysosomes and a reversal in the release of TNF-α, an inflammatory factor induced by a high-fat diet or FFA. These findings suggest that DGSY might improve hepatic function by inhibiting the release of CTSB from lysosomes. CTSB regulation of NF-κB is implicated in many diseases [49,50]. NF-κB is an important transcription factor in the upstream inflammatory signaling pathway of TNF-α [51], and activation of NF-κB is involved in many liver-related diseases [52]. Considering the significant role of NF-κB in liver inflammation, we found that the phosphorylation of the p65 subunit was inhibited after the administration of DGSY. Our data indicate that DGSY might improve NASH by inhibiting hepatic APP protein expression, reducing hepatic lysosomal CTSB release, and suppressing hepatic NF-κB activation.

Our study explores the underlying mechanisms through which DGSY exhibits its effects, providing a deeper understanding of its potential therapeutic application. Considering the significant impact of NASH on public health and the lack of effective therapies, our study is an important step towards developing novel, evidence-based treatment strategies. However, as with all scientific research, this study has limitations. For example, only the mechanism of APP has been explored. The roles of the other proteins in the progression of DGSY therapy have not been established and warrant further investigation. Additionally, we only discussed the mechanism of the DGSY prescription. The specific active ingredients in DGSY responsible for its therapeutic efficacy have yet to be identified and studied [53–55]. We intend to pinpoint and scrutinize the specific active ingredients in DGSY to determine their individual contributions and potential synergistic effects in the improvement of NASH. These subsequent studies will advance our understanding and enhance the potential of DGSY as a therapeutic strategy for NASH.

6. Conclusion

In summary, our study has shown that DGSY significantly improves liver histopathology, reduces hepatic fat deposition, and lowers inflammation, demonstrating a remarkable therapeutic effect on experimental NASH *in vivo* and *in vitro*. It can inhibit the expression of hepatic APP protein, reduce hepatic lysosomal CTSB release, and thereby suppress the activation of hepatic NF-κB. The study provided a more theoretical basis for the future clinical application of DGSY.

Ethics approval and consent to participate

All experimental procedures were performed in accordance with the National Institutes of Health Guidelines for Laboratory Animals and approved by the Animal Ethics Committee of Shanghai University of Chinese Medicine (Permission Number: SZY201710017).

The IRB of Shuguang Hospital affiliated with Shanghai University of TCM considered the databases involved in this study, including the Genecard database, to be public databases. Users can download relevant data for free for research and publish related articles. The study is based on open-source data, so there are no ethical issues and other conflicts of interest. Therefore, they confirmed that the

study did not require ethical approval.

Consent for publication

Not applicable.

Availability of data and materials

Details of data mining, selection, extraction and assessment carried out to support the findings of this study are available from the corresponding author upon request.

Funding

CRediT authorship contribution statement

Siting Gao: Writing – review & editing, Software. **Ziming An:** Investigation, Conceptualization. **Qian Zhang:** Writing – original draft, Investigation. **Qinmei Sun:** Validation, Project administration, Investigation. **Qian Huang:** Software, Resources, Conceptualization. **Lei Shi:** Writing – review & editing, Supervision. **Wei Liu:** Methodology. **Xiaojun Gou:** Supervision, Software, Resources, Funding acquisition. **Yajuan Li:** Validation, Supervision, Funding acquisition. **Xin Xin:** Writing – original draft, Supervision, Data curation, Conceptualization. **Qin Feng:** Supervision, Funding acquisition.

Declaration of competing interest

The authors declare the following financial interests/personal relationships which may be considered as potential competing interests:Qin Feng reports financial support was provided by Shanghai Hospital Development Center. If there are other authors, they declare that they have no known competing financial interests or personal relationships that could have appeared to influence the work reported in this paper.

List of abbreviations

DGSY	Danggui-Shaoyao-San
NASH	nonalcoholic steatohepatitis
APP	amyloid precursor protein
Aβ	amyloid beta
CTSB	cathepsin B
NF-κB	nuclear factor kappa B
FINS	fasting insulin
HFHC	high fat high carbohydrate diet
CON	control
TG	triglycerides
ALT	alanine aminotransferase
AST	aspartate aminotransferase
H&E	hematoxylin and eosin
NAS	non-alcoholic fatty liver disease activity score
IL-6	Interleukin 6
CCL2	C–C motif chemokine ligand 2
TNF-α	tumor necrosis factor alpha
LAMP-1	lysosomal-associated membrane protein 1
PCR	polymerase chain reaction
CETP	cholesteryl ester transfer protein
ApoA1	apolipoprotein A1
ApoA5	apolipoprotein A5
ApoB	apolipoprotein B
LCAT	phosphatidylcholine-sterol acyltransferase
PON1	paraoxonase-1
ApoE	apolipoprotein E

CLU   clusterin
Hp   haptoglobin
FFA   free fatty acid
GADPH   glyceraldehyde 3-phosphate dehydrogenase.

Appendix A. Supplementary data

Supplementary data to this article can be found online at https://doi.org/10.1016/j.heliyon.2024.e34213.

References

[1] M. Eslam, N. Alkhouri, P. Vajro, U. Baumann, R. Weiss, P. Socha, et al., Defining paediatric metabolic (dysfunction)-associated fatty liver disease: an international expert consensus statement, Lancet Gastroenterol Hepatol 6 (10) (2021) 864–873, https://doi.org/10.1016/s2468-1253(21)00183-7.

[2] EASL-EASD-EASO Clinical Practice Guidelines for the management of non-alcoholic fatty liver disease, Diabetologia 59 (6) (2016) 1121–1140, https://doi.org/10.1007/s00125-016-3902-y.

[3] R. Harris, D.J. Harman, T.R. Card, G.P. Aithal, I.N. Guha, Prevalence of clinically significant liver disease within the general population, as defined by non-invasive markers of liver fibrosis: a systematic review, Lancet Gastroenterol Hepatol 2 (4) (2017) 288–297, https://doi.org/10.1016/s2468-1253(16)30205-9.

[4] X. Fu, Q. Wang, Z. Wang, H. Kuang, P. Jiang, Danggui-shaoyao-san: new Hope for Alzheimer's disease, Aging Dis 7 (4) (2016) 502–513, https://doi.org/10.14336/ad.2015.1220.

[5] Y. Zhao, M. Zhao, Z. Wang, C. Zhao, Y. Zhang, M. Wang, Danggui Shaoyao San: chemical characterization and inhibition of oxidative stress and inflammation to treat CCl(4)-induced hepatic fibrosis, J. Ethnopharmacol. 318 (Pt A) (2024) 116870, https://doi.org/10.1016/j.jep.2023.116870.

[6] P. Liu, X. Zhou, H. Zhang, R. Wang, X. Wu, W. Jian, et al., Danggui-shaoyao-san attenuates Cognitive Impairment via the microbiota-gut-brain Axis with regulation of lipid metabolism in Scopolamine-induced Amnesia, Front. Immunol. 13 (2022) 796542, https://doi.org/10.3389/fimmu.2022.796542.

[7] J. Yin, J. Lu, P. Lei, M. He, S. Huang, J. Lv, et al., Danggui-shaoyao-san improves gut microbia dysbiosis and hepatic lipid homeostasis in fructose-fed rats, Front. Pharmacol. 12 (2021) 671708, https://doi.org/10.3389/fphar.2021.671708.

[8] D. Wang, J. Zhou, J. Zhang, M.X. Li, J.G. Qiu, Z.P. Jia, et al., [Effects and HPA Axis related mechanism of kaixin-san and danggui-shaoyao-san on glucose and lipid metabolism in chronic stress rats with high-fat diet], Zhong Yao Cai 38 (9) (2015) 1919–1924.

[9] Y. Sun, Y. Gao, L. Zhou, Y. Lu, Y. Zong, H. Zhu, et al., A multi-target protective effect of Danggui-Shaoyao-San on the vascular endothelium of atherosclerotic mice, BMC Complement Med Ther 23 (1) (2023) 60, https://doi.org/10.1186/s12906-023-03883-3.

[10] C. Yang, Y.S. Mo, H.F. Chen, Y.H. Huang, S.L. Li, H. Wang, et al., The effects of Danggui-Shaoyao-San on neuronal degeneration and amyloidosis in mouse and its molecular mechanism for the treatment of Alzheimer's disease, J. Integr. Neurosci. 20 (2) (2021) 255–264, https://doi.org/10.31083/j.jin2002025.

[11] J. Huang, X. Wang, L. Xie, M. Wu, W. Zhao, Y. Zhang, et al., Extract of Danggui-Shaoyao-San ameliorates cognition deficits by regulating DHA metabolism in APP/PS1 mice, J. Ethnopharmacol. 253 (2020) 112673, https://doi.org/10.1016/j.jep.2020.112673.

[12] Y. Huang, Z.Y. Hu, H. Yuan, L. Shu, G. Liu, S.Y. Qiao, et al., Danggui-shaoyao-san improves learning and memory in female SAMP8 via modulation of estradiol, Evid Based Complement Alternat Med 2014 (2014) 327294, https://doi.org/10.1155/2014/327294.

[13] F.G. Wang, Y. Sun, J. Cao, X.R. Shen, F.W. Liu, S.S. Song, et al., Effects of Danggui-Shaoyao-San on central neuroendocrine and pharmacokinetics in female ovariectomized rats, J. Ethnopharmacol. 316 (2023) 116609, https://doi.org/10.1016/j.jep.2023.116609.

[14] H.W. Lee, J.H. Jun, K.J. Kil, B.S. Ko, C.H. Lee, M.S. Lee, Herbal medicine (Danggui Shaoyao San) for treating primary dysmenorrhea: a systematic review and meta-analysis of randomized controlled trials, Maturitas 85 (2016) 19–26, https://doi.org/10.1016/j.maturitas.2015.11.013.

[15] J. Seo, H. Lee, D. Lee, H.G. Jo, Dangguijagyag-san for primary dysmenorrhea: a PRISMA-compliant systematic review and meta-analysis of randomized-controlled trials, Medicine (Baltim.) 99 (42) (2020) e22761, https://doi.org/10.1097/md.0000000000022761.

[16] H. Xiong, N. Li, L. Zhao, Z. Li, Y. Yu, X. Cui, et al., Integrated serum pharmacochemistry, metabolomics, and network pharmacology to reveal the material basis and mechanism of Danggui shaoyao san in the treatment of primary dysmenorrhea, Front. Pharmacol. 13 (2022) 942955, https://doi.org/10.3389/fphar.2022.942955.

[17] N. Li, X. Cui, C. Ma, Y. Yu, Z. Li, L. Zhao, et al., Uncovering the effects and mechanism of Danggui Shaoyao San intervention on primary dysmenorrhea by serum metabolomics approach, J. Chromatogr., B: Anal. Technol. Biomed. Life Sci. 1209 (2022) 123434, https://doi.org/10.1016/j.jchromb.2022.123434.

[18] M. Qin, T. Zhang, Danggui shaoyaosan attenuates doxorubicin induced nephrotic syndrome through regulating on PI3K/akt pathway, Funct. Integr. Genomics 23 (2) (2023) 148, https://doi.org/10.1007/s10142-023-01071-7.

[19] L. Xiaobing, N. Chunling, C. Wenyu, L. Yan, L. Zhenzhen, Effect of danggui-shaoyao-san-containing serum on the renal tubular epithelial-mesenchymal transition of diabetic nephropathy, Curr. Pharmaceut. Biotechnol. 21 (12) (2020) 1204–1212, https://doi.org/10.2174/1389201021666200416094318.

[20] H. Li, D. Li, G. Zhao, Y. Gao, J. Ke, Effects of Danggui-Shaoyao-San on depression- and anxiety-like behaviors of rats induced by experimental tooth movement, J. Orofac. Orthop. 83 (1) (2022) 23–33, https://doi.org/10.1007/s00056-021-00323-0.

[21] M. Xia, N. Ai, J. Pang, Preliminary exploration of clinical efficacy and pharmacological mechanism of modified danggui-shaoyao san in the treatment of depression in patients with chronic kidney disease, Drug Des. Dev. Ther. 16 (2022) 3975–3989, https://doi.org/10.2147/dddt.S387677.

[22] W. Guo, X. Yao, R. Cui, W. Yang, L. Wang, Mechanisms of paeoniaceae action as an antidepressant, Front. Pharmacol. 13 (2022) 934199, https://doi.org/10.3389/fphar.2022.934199.

[23] Q. Huang, Z. An, X. Xin, Q. Sun, S. Gao, S. Lv, et al., Effectiveness and safety analysis of Danggui Shaoyao Powder for the treatment of non-alcoholic fatty liver disease: study protocol for a randomized, double-blind, placebo-controlled clinical trial, BMC Complement Med Ther 23 (1) (2023) 126, https://doi.org/10.1186/s12906-023-03948-3.

[24] F. Cheng, Q. Li, J. Wang, F. Zeng, Y. Zhang, Investigation of the potential mechanism of Danggui shaoyao san for the treatment of non-alcoholic fatty liver disease (NAFLD) with network pharmacology and molecular docking, Curr. Comput. Aided Drug Des. 18 (4) (2022) 258–270, https://doi.org/10.2174/1573409918666220815093324.

[25] Z.M. Younossi, V. Ratziu, R. Loomba, M. Rinella, Q.M. Anstee, Z. Goodman, et al., Obeticholic acid for the treatment of non-alcoholic steatohepatitis: interim analysis from a multicentre, randomised, placebo-controlled phase 3 trial, Lancet 394 (10215) (2019) 2184–2196, https://doi.org/10.1016/s0140-6736(19)33041-7.

[26] H. Tang, J. Wang, Y. Fang, Y. Yin, W. Liu, Y. Hu, et al., Hepatic transcriptome discloses the potential targets of Xuefu Zhuyu Decoction ameliorating non-alcoholic fatty liver disease induced by high-fat diet, J Tradit Complement Med 14 (2) (2024) 135–147, https://doi.org/10.1016/j.jtcme.2023.07.008.

[27] X. Xin, B.Y. Cai, C. Chen, H.J. Tian, X. Wang, Y.Y. Hu, et al., High-trans fatty acid and high-sugar diets can cause mice with non-alcoholic steatohepatitis with liver fibrosis and potential pathogenesis, Nutr. Metab. 17 (2020) 40, https://doi.org/10.1186/s12986-020-00462-y.

[28] J.H.H.X. Huang, Z.Y. Chen, Q.S. Zheng, R.Y. Sun, Dose conversion among different animals and between animals and humans in pharmacological studies, Chin. J. Clin. Pharmacol. Therapeut. 9 (9) (2004) 3.

[29] J. He, Y. Jin, C. He, Z. Li, W. Yu, J. Zhou, et al., Danggui Shaoyao San: comprehensive modulation of the microbiota-gut-brain axis for attenuating Alzheimer's disease-related pathology, Front. Pharmacol. 14 (2023) 1338804, https://doi.org/10.3389/fphar.2023.1338804.

[30] L.X. Zhang, J. Dong, H. Wei, S.H. Shi, A.P. Lu, G.M. Deng, et al., TCMSID: a simplified integrated database for drug discovery from traditional Chinese medicine, J. Cheminf. 14 (1) (2022) 89, https://doi.org/10.1186/s13321-022-00670-z.

[31] M. Safran, I. Dalah, J. Alexander, N. Rosen, T. Iny Stein, M. Shmoish, et al., GeneCards Version 3: the human gene integrator, Database 2010 (2010) baq020, https://doi.org/10.1093/database/baq020.

[32] A. Daina, O. Michielin, V. Zoete, SwissTargetPrediction: updated data and new features for efficient prediction of protein targets of small molecules, Nucleic Acids Res. 47 (W1) (2019) W357–W364, https://doi.org/10.1093/nar/gkz382.

[33] C.W. Hsia, M.Y. Ho, H.A. Shui, C.B. Tsai, M.J. Tseng, Analysis of dermal papilla cell interactome using STRING database to profile the ex vivo hair growth inhibition effect of a vinca alkaloid drug, colchicine, Int. J. Mol. Sci. 16 (2) (2015) 3579–3598, https://doi.org/10.3390/ijms16023579.

[34] Y. Zhao, X. He, X. Shi, C. Huang, J. Liu, S. Zhou, et al., Association between serum amyloid A and obesity: a meta-analysis and systematic review, Inflamm. Res. 59 (5) (2010) 323–334, https://doi.org/10.1007/s00011-010-0163-y.

[35] M. Hefner, V. Baliga, K. Amphay, D. Ramos, V. Hegde, Cardiometabolic modification of amyloid beta in Alzheimer's disease pathology, Front. Aging Neurosci. 13 (2021) 721858, https://doi.org/10.3389/fnagi.2021.721858.

[36] Y. Guo, Q. Wang, S. Chen, C. Xu, Functions of amyloid precursor protein in metabolic diseases, Metabolism 115 (2021) 154454, https://doi.org/10.1016/j.metabol.2020.154454.

[37] G. Weinstein, A. O'Donnell, K. Davis-Plourde, S. Zelber-Sagi, S. Ghosh, C.S. DeCarli, et al., Non-alcoholic fatty liver disease, liver fibrosis, and regional amyloid-β and tau pathology in middle-aged adults: the framingham study, J Alzheimers Dis 86 (3) (2022) 1371–1383, https://doi.org/10.3233/jad-215409.

[38] R. Sudo, F. Sato, T. Azechi, H. Wachi, 7-Ketocholesterol-induced lysosomal dysfunction exacerbates vascular smooth muscle cell calcification via oxidative stress, Gene Cell. 20 (12) (2015) 982–991, https://doi.org/10.1111/gtc.12301.

[39] M. Goeritzer, N. Vujic, S. Schlager, P.G. Chandak, M. Korbelius, B. Gottschalk, et al., Active autophagy but not lipophagy in macrophages with defective lipolysis, Biochim. Biophys. Acta 1851 (10) (2015) 1304–1316, https://doi.org/10.1016/j.bbalip.2015.06.005.

[40] Y. Liu, R. Palanivel, E. Rai, M. Park, T.V. Gabor, M.P. Scheid, et al., Adiponectin stimulates autophagy and reduces oxidative stress to enhance insulin sensitivity during high-fat diet feeding in mice, Diabetes 64 (1) (2015) 36–48, https://doi.org/10.2337/db14-0267.

[41] B.F. Li, S. Huang, K. Wu, Y. Liu, Altered cathepsin B expression as a diagnostic marker of skeletal muscle insulin resistance in type 2 diabetes, ACS Biomater. Sci. Eng. 9 (5) (2023) 2731–2740, https://doi.org/10.1021/acsbiomaterials.3c00078.

[42] P. Nagakannan, M.I. Islam, M. Conrad, E. Eftekharpour, Cathepsin B is an executioner of ferroptosis, Biochim. Biophys. Acta Mol. Cell Res. 1868 (3) (2021) 118928, https://doi.org/10.1016/j.bbamcr.2020.118928.

[43] A.E. Feldstein, N.W. Werneburg, Z. Li, S.F. Bronk, G.J. Gores, Bax inhibition protects against free fatty acid-induced lysosomal permeabilization, Am. J. Physiol. Gastrointest. Liver Physiol. 290 (6) (2006) G1339–G1346, https://doi.org/10.1152/ajpgi.00509.2005.

[44] Y.A. An, C. Crewe, I.W. Asterholm, K. Sun, S. Chen, F. Zhang, et al., Dysregulation of amyloid precursor protein impairs adipose tissue mitochondrial function and promotes obesity, Nat. Metab. 1 (12) (2019) 1243–1257, https://doi.org/10.1038/s42255-019-0149-1.

[45] Y.W. Zhang, R. Thompson, H. Zhang, H. Xu, APP processing in Alzheimer's disease, Mol. Brain 4 (2011) 3, https://doi.org/10.1186/1756-6606-4-3.

[46] A. Halle, V. Hornung, G.C. Petzold, C.R. Stewart, B.G. Monks, T. Reinheckel, et al., The NALP3 inflammasome is involved in the innate immune response to amyloid-beta, Nat. Immunol. 9 (8) (2008) 857–865, https://doi.org/10.1038/ni.1636.

[47] M.A. de Castro, G. Bunt, F.S. Wouters, Cathepsin B launches an apoptotic exit effort upon cell death-associated disruption of lysosomes, Cell Death Dis. 2 (2016) 16012, https://doi.org/10.1038/cddiscovery.2016.12.

[48] A.E. Feldstein, N.W. Werneburg, A. Canbay, M.E. Guicciardi, S.F. Bronk, R. Rydzewski, et al., Free fatty acids promote hepatic lipotoxicity by stimulating TNF-alpha expression via a lysosomal pathway, Hepatology 40 (1) (2004) 185–194, https://doi.org/10.1002/hep.20283.

[49] X. Li, Z. Wu, J. Ni, Y. Liu, J. Meng, W. Yu, et al., Cathepsin B regulates collagen expression by fibroblasts via prolonging TLR2/NF-κB activation, Oxid. Med. Cell. Longev. 2016 (2016) 7894247, https://doi.org/10.1155/2016/7894247.

[50] M. Sendler, F.U. Weiss, J. Golchert, G. Homuth, C. van den Brandt, U.M. Mahajan, et al., Cathepsin B-mediated activation of trypsinogen in endocytosing macrophages increases severity of pancreatitis in mice, Gastroenterology 154 (3) (2018) 704–718, https://doi.org/10.1053/j.gastro.2017.10.018, e10.

[51] G. Gloire, J. Piette, Redox regulation of nuclear post-translational modifications during NF-kappaB activation, Antioxidants Redox Signal. 11 (9) (2009) 2209–2222, https://doi.org/10.1089/ars.2009.2463.

[52] A.M. Elsharkawy, D.A. Mann, Nuclear factor-kappaB and the hepatic inflammation-fibrosis-cancer axis, Hepatology 46 (2) (2007) 590–597, https://doi.org/10.1002/hep.21802.

[53] Q. Meng, X.P. Duan, C.Y. Wang, Z.H. Liu, P.Y. Sun, X.K. Huo, et al., Alisol B 23-acetate protects against non-alcoholic steatohepatitis in mice via farnesoid X receptor activation, Acta Pharmacol. Sin. 38 (1) (2017) 69–79, https://doi.org/10.1038/aps.2016.119.

[54] Z. Ma, L. Chu, H. Liu, J. Li, Y. Zhang, W. Liu, et al., Paeoniflorin alleviates non-alcoholic steatohepatitis in rats: involvement with the ROCK/NF-κB pathway, Int. Immunopharm. 38 (2016) 377–384, https://doi.org/10.1016/j.intimp.2016.06.023.

[55] G.Y. Sasaki, J. Li, M.J. Cichon, R.E. Kopec, R.S. Bruno, Catechin-rich green tea extract and the loss-of-TLR4 signaling differentially alter the hepatic metabolome in mice with nonalcoholic steatohepatitis, Mol. Nutr. Food Res. 65 (2) (2021) e2000998, https://doi.org/10.1002/mnfr.202000998.